Astronomy & Astrophysics manuscript no. paper
March 22, 2023

My paper on the cosmic microwave background and formation of structures in our Universe

V. A. Vikenes[1]

Institute of Theoretical Astrophysics, University of Oslo, 0315 Oslo, Norway
e-mail: v.a.vikenes@astro.uio.no

March 22, 2023

ABSTRACT

The code for this project can be found on my GitHub repository: https://github.com/Vikenes/AST5220/

Key words. cosmic microwave background – large-scale structure of Universe

1. Introduction

Write an introduction here. Give context to the paper. Citations to relevant papers. You only need to do this in the end for the last milestone.

2. Milestone I

In this section we will examine the evolution of the Universe's uniform background. Our primary objective is to develop methods for computing the Hubble parameter and related time- and distance measures. These methods provide a first step towards further investigations and modelling of the early Universe. To compute the background cosmology, we will solve ordinary differential equations (ODEs) numerically, using cosmological parameters obtained from the Planck Collaboration [1]. The parameters we will use are listed in Eq. (A.1) in Appendix A. One crucial aspect in the process is validating our model. We will therefore develop some simple methods for comparing our result. This will mainly involve considering simplified cases where analytical solutions can be obtained.

Our primary focus in this section concerns methods where the cosmological parameters are given from the start. Another interesting aspect is to use data to constrain cosmological parameters. To do this, we will use data from supernova observations [2], containing luminosity distance associated with different values of redshift. By employing the numerical methods we develop initially, we will try to estimate optimal values of three cosmological parameters, by implement a simple Markov chain Monte Carlo (MCMC) algorithm. The parameters we will be sampling are h, Ω_{m0} and Ω_{k0}. From these results, we will investigate confidence regions of Ω_{m0} and $\Omega_{\Lambda 0}$, and try to estimate a probability distribution function (PDF) for the Hubble parameter.

The code for this milestone can be found on my GitHub repository: https://github.com/Vikenes/AST5220/tree/main/projects/milestone1

2.1. Theory

2.1.1. Density parameters and Hubble factor

The Friedmann equation can be written in terms of density parameters, $\Omega_i \equiv \rho_i/\rho_c$, where $\rho_c \equiv 3H^2/8\pi G$ is the critical density. The density of a given species, i, evolves as [3, Eq. (2.61)]

$$\rho_i(t) \propto a(t)^{-3(1+w_i)}, \tag{1}$$

where we have assumed that the equation of state (EoS) parameter, $w_i \equiv P_i/\rho_i$ [3, Eq. 2.60], is constant. P_i denotes the pressure of the species. We will limit ourselves to consider three types of species in this report: matter, radiation and dark energy. We will only consider baryons and cold dark matter (CDM) for the matter component, which we express as $\Omega_{m0} = \Omega_{b0} + \Omega_{\rm CDM0}$. The subscript 0 is used to refer to today's value. The radiation component we consider is $\Omega_{r0} = \Omega_{\gamma 0} + \Omega_{\nu 0}$, corresponding to photons and neutrinos, respectively. For the dark energy, we only have the cosmological constant $\Omega_{\Lambda 0}$.

Matter, radiation and dark energy have densities evolving according to Eq. (1) with $w_i = 0$, $1/3$ and -1, respectively. Neutrinos having $w = 1/3$ only holds since we will assume that the neutrinos are massless. Curvature can be described by $w_i = -1/3$, with $\Omega_{k0} \equiv -kc^2/H_0^2$. The parameter k represents the curvature of the Universe, where $k = 0$ corresponds to a flat Universe. With these parameters, the Friedmann Equation can be written as [3, Eq. (3.14)]

$$H = H_0 \sqrt{\Omega_{m0} a^{-3} + \Omega_{r0} a^{-4} + \Omega_{k0} a^{-2} + \Omega_{\Lambda 0}}, \tag{2}$$

where $H \equiv \dot{a}/a$ is the Hubble parameter, with the dot denoting a derivative with respect to cosmic time, t. For the radiation, $\Omega_{\gamma 0}$ and $\Omega_{\nu 0}$ follow from the temperature of the CMB today, $T_{\rm CMB0}$, and the effective number of massless neutrinos, $N_{\rm eff}$. They are given by

$$\Omega_{\gamma 0} = 2 \cdot \frac{\pi^2}{30} \frac{(k_b T_{\rm CMB0})^4}{\hbar^3 c^5} \cdot \frac{8\pi G}{3H_0^2}, \tag{3}$$

$$\Omega_{\nu 0} = N_{\rm eff} \cdot \frac{7}{8} \cdot \left(\frac{4}{11}\right)^{4/3} \Omega_{\gamma 0}. \tag{4}$$

The value of $\Omega_{\Lambda 0}$ is fixed by the requirement that $H(a = 1) = H_0$, yielding

$$\Omega_{\Lambda 0} = 1 - (\Omega_{m0} + \Omega_{r0} + \Omega_{k0}). \tag{5}$$

We also introduce the scaled Hubble factor, $\mathcal{H} \equiv aH$. Rather than working with the scale factor, $a(t)$, we will mainly be working with the logarithm of the scale factor

$$x \equiv \ln a, \quad ' \equiv \frac{\mathrm{d}}{\mathrm{d}x}. \tag{6}$$

The resulting expression for $\mathcal{H}(x)$ is thus

$$\mathcal{H}(x) = H_0 \sqrt{\Omega_{m0} e^{-x} + \Omega_{r0} e^{-2x} + \Omega_{k0} + \Omega_{\Lambda 0} e^{2x}}. \tag{7}$$

This form of the Hubble factor is the one we will focus on for the majority of this report. In terms of $\mathcal{H}(x)$, the value of the density parameters can be obtained at any given x, with

$$\Omega_k(x) = \frac{\Omega_{k0}}{\mathcal{H}(x)^2/H_0^2}, \tag{8}$$

$$\Omega_m(x) = \frac{\Omega_{m0}}{e^x \mathcal{H}(x)^2/H_0^2}, \tag{9}$$

$$\Omega_r(x) = \frac{\Omega_{r0}}{e^{2x} \mathcal{H}(x)^2/H_0^2}, \tag{10}$$

$$\Omega_\Lambda(x) = \frac{\Omega_{\Lambda 0}}{e^{-2x} \mathcal{H}(x)^2/H_0^2}, \tag{11}$$

From these expressions, we can identify the epochs during which the Universe was dominated by an equal amount of matter and radiation, and by an equal amount of matter and dark energy. These epochs are defined by the time when $\Omega_m = \Omega_r$ and $\Omega_m = \Omega_\Lambda$, respectively, and are a valuable asset towards understanding the physics governing the evolution of the Universe. Another time of interest is the onset of acceleration, defined as the time when $\ddot{a} = 0$. In terms of $\mathcal{H}$ and x, this corresponds to

$$\ddot{a} = \frac{\mathrm{d}x}{\mathrm{d}t}\frac{\mathrm{d}\dot{a}}{\mathrm{d}x} = \frac{\mathrm{d}\ln a}{\mathrm{d}t}\frac{\mathrm{d}\mathcal{H}(x)}{\mathrm{d}x} = e^{-x}\mathcal{H}(x)\frac{\mathrm{d}\mathcal{H}(x)}{\mathrm{d}x}. \tag{12}$$

In Sect. 2.1.4 we will derive an expression for $\mathcal{H}'(x)$.

2.1.2. Conformal time

We now want to relate the Hubble factor to some time variables. The main one we will consider is the conformal time, η. It is a measure of the distance light has been able to travel since $t = 0$, where t is the cosmic time. Using its definition in terms of t [3, Eq. (2.90)], we can express it in terms of x as

$$\eta = \int_0^t \frac{c\,\mathrm{d}t'}{a(t')} = \int_{-\infty}^{x'} \frac{c\,\mathrm{d}x'}{\mathcal{H}(x')}. \tag{13}$$

This leads us to the following differential equation that we will solve numerically

$$\frac{\mathrm{d}\eta}{\mathrm{d}x} = \frac{c}{\mathcal{H}(x)}. \tag{14}$$

The initial condition we have is $\eta(-\infty) = 0$. Noting from Eq. (7) that $\mathcal{H}(x) \to H_0\sqrt{\Omega_{r0}}e^{-x}$ as $x \to -\infty$, we get an analytical approximation for the initial condition of η at early times

$$\eta(x_{\mathrm{start}}) \approx \int_{-\infty}^{x_{\mathrm{start}}} \frac{c\,\mathrm{d}x'}{H_0\sqrt{\Omega_{r0}}} e^{x'} = \frac{c}{\mathcal{H}(x_{\mathrm{start}})}. \tag{15}$$

Note that $\eta(x)\mathcal{H}(x)/c \to 1$ at low x, which provides a natural way of validating our implementation.

For the cosmic time, t, starting from $H = \dot{a}/a$ and applying the chain rule yields the desired differential equation for $t(x)$, which we will solve numerically,

$$\frac{\mathrm{d}t}{\mathrm{d}x} = \frac{1}{H(x)}. \tag{16}$$

To get an initial condition for t, we consider the radiation dominating era, with the following integral expression

$$t(x) = \int_{-\infty}^{x} \frac{\mathrm{d}x'}{H(x')}. \tag{17}$$

Comparing with Eq. (15), we see that the two integrands only differ by a factor e^x. The initial condition for t is therefore easily seen to be

$$t(x_{\mathrm{start}}) = \frac{1}{2H(x_{\mathrm{start}})}. \tag{18}$$

2.1.3. Distance measures

The supernova data we will study has distances measured in terms of luminosity distance, d_L. Expressing it in terms of the angular distance, $d_A = ar$, it becomes

$$d_L(a) = \frac{d_A}{a^2} = \frac{r}{a} \implies d_L(x) = e^{-x} r. \tag{19}$$

Here, r represents the radial coordinate of the emitted photon. To get an expression for r, we consider a photon's line-element in spherical coordinates,

$$ds^2 = -c^2 dt^2 + a^2\left(\frac{dr^2}{1-kr^2} + r^2 d\theta^2 + r^2 \sin^2\theta d\phi^2\right). \tag{20}$$

For photons travelling radially towards us, we have $\mathrm{d}\theta = \mathrm{d}\phi = 0$. Since $ds^2 = 0$ for photons, integrating the line-element of a photon emitted at, (t, r), reaching an observer at $(t_0, 0)$, yields

$$\int_0^r \frac{\mathrm{d}r'}{\sqrt{1-kr'}} = \int_t^{t_0} \frac{c\,\mathrm{d}t}{a}. \tag{21}$$

The RHS of Eq. (21) is known as the co-moving distance, χ, which in terms of conformal time is given as

$$\chi = \int_t^{t_0} \frac{c\,\mathrm{d}t}{a} = \int_x^0 \frac{c\,\mathrm{d}x'}{\mathcal{H}(x')} = \eta(0) - \eta(x). \tag{22}$$

Solving Eq. (21) with respect to r, we get

$$r = \begin{cases} \chi \cdot \frac{\sin\left(\sqrt{|\Omega_{k0}|}H_0\chi/c\right)}{\left(\sqrt{|\Omega_{k0}|}H_0\chi/c\right)}, & \Omega_{k0} < 0, \\ \chi, & \Omega_{k0} = 0, \\ \chi \cdot \frac{\sinh\left(\sqrt{|\Omega_{k0}|}H_0\chi/c\right)}{\left(\sqrt{|\Omega_{k0}|}H_0\chi/c\right)}, & \Omega_{k0} > 0. \end{cases} \tag{23}$$

Eq. (19) can now be used to compute d_L, and the expression to use depends on the curvature.

2.1.4. Analytical solutions

In Sect. 2.1.2 we discussed how $\eta(x)$ can be used to test our implementation in the radiation dominating era. To test our solutions in other regimes, we will need the first and second derivative of $\mathcal{H}(x)$. To simplify the resulting expressions, we define the function, $g(x)$, as the derivative of the term inside the square root in Eq. (7), namely

$$g(x) \equiv -\Omega_{m0}e^{-x} - 2\Omega_{r0}e^{-2x} + 2\Omega_{\Lambda 0}e^{2x}. \tag{24}$$

The first two derivatives of $\mathcal{H}(x)$ are easily seen to be

$$\frac{\mathrm{d}\mathcal{H}(x)}{\mathrm{d}x} = \frac{H_0^2}{2\mathcal{H}(x)}g(x), \tag{25}$$

$$\frac{\mathrm{d}^2\mathcal{H}(x)}{\mathrm{d}x^2} = \frac{H_0^2}{2\mathcal{H}(x)}\left[g'(x) - \frac{1}{2}\left(\frac{H_0 g(x)}{\mathcal{H}(x)}\right)^2\right]. \tag{26}$$

Now we will consider the situation where the Universe is dominated by a single fluid with a constant EoS parameter, w. In that case we have $H(t)^2 \propto \rho_i(t)^2$ [3, Eq. (3.13)]. Using Eq. (1), the Hubble parameter expressed in terms of w_i becomes

$$H(t)^2 \propto a^{-3(1+w)} \implies \mathcal{H}(x) = c_1 e^{-\frac{3}{2}(1+w)x}, \tag{27}$$

where c_1 is some constant. The reason for doing this, is that both c_1 and the exponential factor drops out when we consider $\mathcal{H}'(x)/\mathcal{H}(x)$ and $\mathcal{H}''(x)/\mathcal{H}(x)$. For different values of w_i, $\mathcal{H}'(x)/\mathcal{H}(x)$ becomes

$$\frac{1}{\mathcal{H}(x)}\frac{\mathrm{d}\mathcal{H}}{\mathrm{d}x} = -\frac{1+3w}{2} = \begin{cases} -1, & w = 1/3, \\ -1/2, & w = 0, \\ 1, & w = -1. \end{cases} \tag{28}$$

Similarly, the expression for $\mathcal{H}''(x)/\mathcal{H}(x)$ becomes

$$\frac{1}{\mathcal{H}(x)^2}\frac{\mathrm{d}^2\mathcal{H}}{\mathrm{d}x^2} = \frac{(1+3w)^2}{2} = \begin{cases} 1, & w = 1/3 \\ 1/4, & w = 0 \\ 1, & w = -1 \end{cases} \tag{29}$$

Equations (28) and (29) offer a means to evaluate the accuracy of our numerical solution at different regimes. Each density parameter evolve differently with x, as seen from Eqs. (8)-(11). Certain ranges of x-values will therefore closely resemble a Universe that is dominated by a single fluid. By computing $\mathcal{H}$, $\mathcal{H}'$, and $\mathcal{H}''$, we can examine whether these quantities exhibit the expected behaviour. This allows us to assess the validity of our model and ensure that it is consistent with the underlying physical principles.

2.2. Implementation details

To solve the differential equations for η and t (Eq. (14) and (16)) we use the C++ library GSL [4], and use their Runge-Kutta4 solver. From the solution we create a spline of the results for the given x domain we have considered.

We will consider three different ranges of x-values. For the initial testing, we will use $x \in [\ln 10^{-10}, 5]$. For fitting cosmological parameters to the supernova data, we will use $x \in [\ln 10^{-2}, 0]$. When we want to estimate important times during the cosmic evolution, we will consider $x \in [-10, 1]$, for increased resolution, as the result may vary by a noticeable amount between step sizes. In all cases, we use $N_x = 10^5$ number of points.

The cosmological parameters we consider assume $\Omega_{k0} = 0$. In Sect. 2.2.1 we discuss how we will use supernova data to estimate a value for Ω_{k0}. Curvature is therefore implemented in all the relevant methods, but we set $\Omega_{k0} = 0$ when we're not dealing with supernova fitting.

2.2.1. Supernova fitting and parameter sampling

The supernova data we will use contains $N = 31$ data points of luminosity distance, $d_L^{\mathrm{obs}}(z_i)$, with associated measurement errors, σ_i, at different redshifts, $z_i \in [0.01, 1.30]$. This corresponds to $x \sim [-9.95 \cdot 10^{-3}, -0.833]$. Using these measurements, we want to constrain the three-dimensional parameter space

$$C = \left\{\hat{h},\ \hat{\Omega}_{m0},\ \hat{\Omega}_{k0}\right\}, \tag{30}$$

where the hat is used to distinguish the estimated parameters from the fiducial ones. We use $\Omega_{b0} = 0.05$ for this analysis, so $\hat{\Omega}_{m0}$ enters via $\Omega_{\mathrm{CDM}0} = \hat{\Omega}_{m0} - \Omega_{b0}$. Additionally, the neutrinos are not relevant at the small scale considered here, and we therefore set $N_{\mathrm{eff}} = 0$ for this analysis.

We will assume that the measurements at different redshifts are normal distributed and uncorrelated. The likelihood function is then given by $L \propto e^{-\chi^2/2}$, where

$$\chi^2(C) = \sum_{i=1}^{N} \frac{[d_L(z_i, C) - d_L^{\mathrm{obs}}(z_i)]^2}{\sigma_i^2}, \tag{31}$$

is the function we want to minimize. To do this, we will sample parameter values randomly by a Markov chain Monte Carlo (MCMC) process. We also restrict the parameter space to sample, with the following limits:

$$\begin{aligned} 0.5 &< \hat{h} < 1.5, \\ 0 &< \hat{\Omega}_{m0} < 1, \\ -1 &< \hat{\Omega}_{k0} < 1. \end{aligned} \tag{32}$$

To generate a new sample, we update each parameter by generating a random number $P \sim \mathcal{N}(0, 1)$, and multiplying it by a step size. We will use step sizes of $\Delta\hat{h} = 0.007$, $\Delta\hat{\Omega}_{m0} = 0.05$, $\Delta\hat{\Omega}_{k0} = 0.05$. To determine whether a new configuration should be included in the sample we use the Metropolis algorithm, where we always accept a state if it yields a lower value of χ^2 compared to the previous state that was accepted. If the new value of χ^2 is greater than the old one, we accept it if the ratio of the likelihood functions $L(\chi^2_{\mathrm{new}})/L(\chi^2_{\mathrm{old}}) > p$, where $p \sim \mathcal{U}(0, 1)$. We continue drawing samples until we get a total of $\hat{n} = 10^4$ samples. For the samples generated, we omit the first 1000 samples of the chain from our analysis.

With our generated samples, we can use the best fit, χ^2_{min}, to find the 1σ and 2σ confidence regions. For the χ^2 distribution with 3 parameters, these regions are given by $\chi^2 - \chi^2_{\mathrm{min}} < 3.53$ and $\chi^2 - \chi^2_{\mathrm{min}} < 8.02$, respectively. We will plot the 1σ and 2σ constraint in the $(\Omega_{m0}, \Omega_{\Lambda 0})$ plane. Since $\Omega_{r0} < 10^{-4}$, $\Omega_{\Lambda 0}$ can be approximated well by $\Omega_{\Lambda 0} = 1 - \Omega_{m0}$. After that we will plot the posterior probability distribution function (PDF) for H_0.

To compare our fit with the Planck data, we will plot $d_L^{\mathrm{obs}}(z_i)$ together with $d_L^{\mathrm{fit}}(z)$ and $d_L^{\mathrm{Planck}}(z)$. We obtain the former by solving the background cosmology with h, Ω_{m0}, Ω_{k0} replaced by the configuration $\hat{h}$, $\hat{\Omega}_{m0}$, $\hat{\Omega}_{k0}$ that yielded the lowest value of χ^2.

2.3. Results

In this section we present the results from our numerical simulations. Most of our results concern the evolution of various parameters as a function of x. Whenever it's relevant for interpreting and understanding the plot, we mark the point where we have matter-radiation equality and matter-dark energy equality, corresponding to $\Omega_m = \Omega_r$ and $\Omega_m = \Omega_\Lambda$, respectively. These points can be seen directly in Fig. 5.

2.3.1. Analytical and numerical comparisons

The dimensionless quantity $\eta\mathcal{H}/c$ is shown in Fig. 1. At the lowest values of $x \lesssim -10$, we see that $\eta\mathcal{H}/c = 1$, as expected. Slightly before matter-radiation equality takes place, we see a slight increase towards higher x. As we approach higher x, Ω_Λ starts dominating, and the solution eventually diverges, as expected.

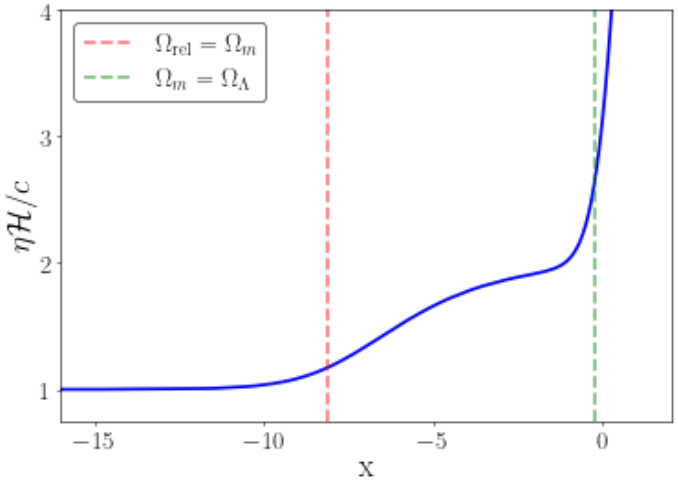

Fig. 1. The dimensionless quantity $\eta\mathcal{H}/c$ as a function of x. At low x it has a value of 1, as expected. The most significant changes occur near regions where there is a change in which density parameter is dominating.

In Fig. 2 we have plotted $\mathcal{H}'/\mathcal{H}$ and $\mathcal{H}''/\mathcal{H}$, where we include the analytical approximation from Eq. (28) and Eq. (29), respectively. The different values of w are drawn over the whole range of x where their related density parameter is larger than the other two. This is done for visibility purposes, and we only expect approximations to be reasonable whenever a density parameter is close to 1.

Towards the smallest values of x we see that both quantities are well approximated by the analytical solutions for $w = 1/3$. As we reach $x \gtrsim 12$, matter becomes increasingly dominant, and the solution deviates from being purely dominated by a $w = 1/3$ fluid. Towards the highest values of x, we see that both quantities reach a constant value of 1 for $w = -1$. At higher values of x, we know that both $\Omega_m(x)$ and $\Omega_r(x)$ should vanish, eventually, while $\Omega_\Lambda \to 1$. This behaviour is thus present in our implementation. When matter dominates, we see that both functions exhibit inferior agreement with the approximations compared to the other regimes. This can be understood from Fig. 5, where the vanishing contribution of Ω_r occurs around the same time as Ω_Λ starts contributing. The maximum value reached for this particular configuration is $\Omega_m \approx 0.995$. Nonetheless, significant deviations from the analytical solutions are not evident.

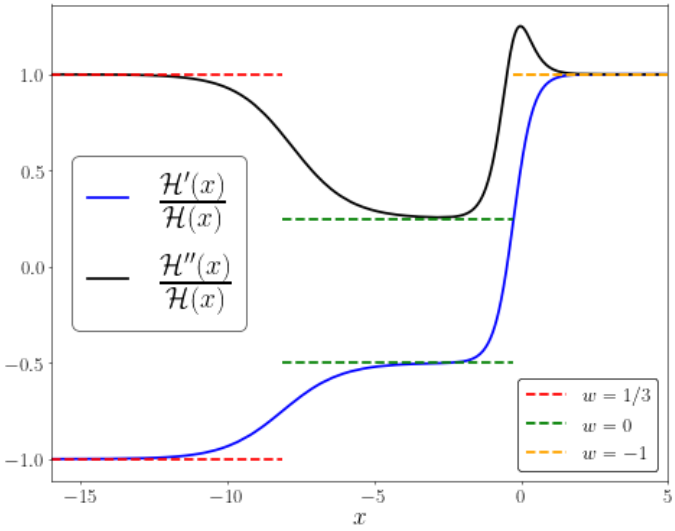

Fig. 2. $\mathcal{H}'/\mathcal{H}$ and $\mathcal{H}''/\mathcal{H}$ compared with analytical expressions in the case a single fluid with a given EoS parameter, w, shown by the dashed lines. The transition between the dashed lines are chosen as the corresponding epochs of equality.

2.3.2. Hubble factor and time variables

Having checked that our implementation is physical, we now proceed by studying the evolution of the background, starting with a plot of the conformal Hubble factor, $\mathcal{H}(x)$, show in Fig. 3.

The local minima taking place before matter-dark energy equality corresponds to the onset of acceleration, where $\ddot{a} = 0$. For $x > 0$, Ω_Λ will dominate the conformal Hubble factor, where we have $\mathcal{H}(x) \propto e^x$, as seen from Eq. (7).

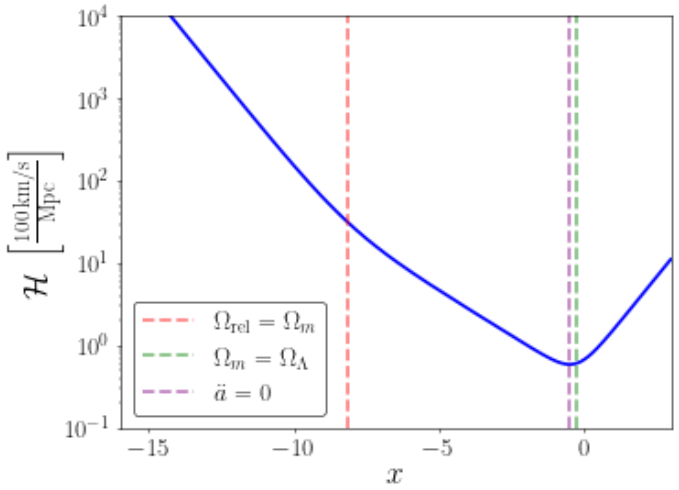

Fig. 3. Evolution of the conformal Hubble factor. The minimum point marks the onset of acceleration, after which, dark energy dominates its evolution.

The evolution of $\eta(x)$ and $t(x)$ is shown in Fig. 4. At high values of x, the e^x dependence of $\mathcal{H}(x)$ causes $\eta(x)$ to grow as e^{-x} at late times, suppressing its growth. The cosmic time, on the other hand, does not have an exponential dependence in the integrand at high values of x. This yields the linear growth we see at late times. The different x-dependece of t and η results in the two quantities to be approximately equal at $x \sim 2.75$.

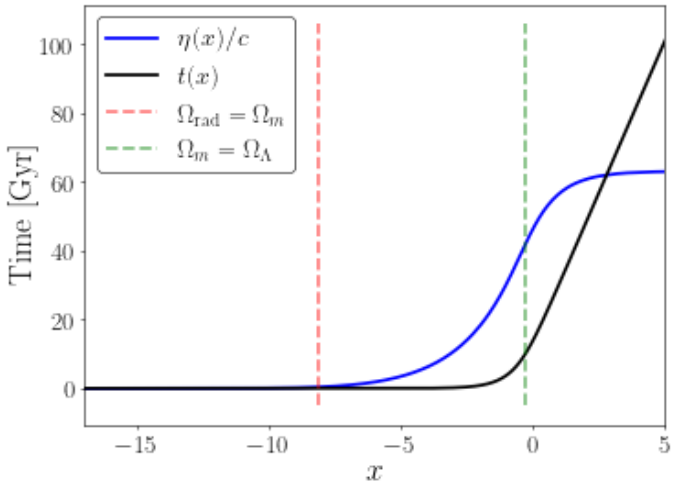

Fig. 4. The cosmic time, t and conformal time η/c. We emphasize that $\eta \neq t$ at small x, but the difference is discernable on the scale considered.

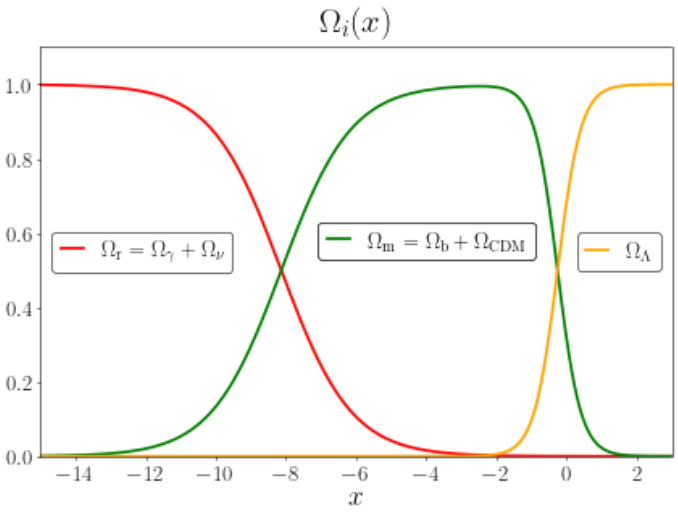

Fig. 5. Evolution of the density parameters over time. The points where $\Omega_m = \Omega_r$ marks the epoch of matter-radiation equality, and the intersection between Ω_m and Ω_Λ marks the epoch of matter-dark energy equality. The sum of the three quantities never exceed 1, as expected.

2.3.3. Supernova fitting

A plot showing the luminosity distance as a function of redshift is shown in Fig. 6, where we plot $d_L(z)/z$ to better compare the simulations with the data. There is a noticeable discrepancy between the simulated luminosity distance and the data, with most redshifts causing the simulation to fall outside the uncertainties.

The 1σ and 2σ confidence regions in the $\Omega_\Lambda - \Omega_m$ plane is shown in Fig. 7. In the figure we have also indicated the parameter configuration for a flat Universe. A majority of the configurations seem to favour a non-flat Universe, with $\Omega_{k0} \approx 0.0674$. This could be a result of local variations in the gravitational field at small scales.

The posterior PDF of H_0 is shown in Fig. 8, where we have included the resulting Gaussian distribution from the mean and variance of the sampled H_0 values. This shows further discrepancy from the value of $H_0 = 67\,\mathrm{km/s/Mpc}$, given by Planck, while the mean value we obtain is $\hat{H}_0 = 70.1\,\mathrm{km/s/Mpc}$, with a corresponding standard deviation of $\hat{\sigma}_{H_0} = 0.64\,\mathrm{km/s/Mpc}$.

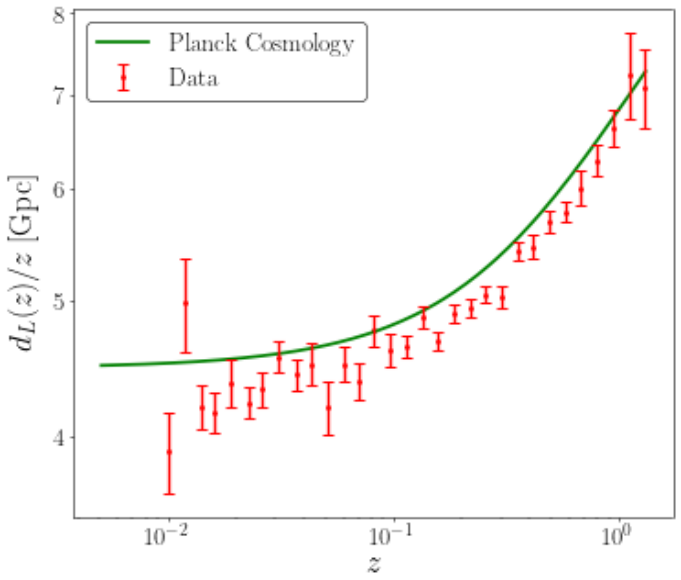

Fig. 6. Supernova data compared with the predicted luminosity distance obtained from simulations using Planck cosmology. Note that we use a logarithmic scale for the y-axis.

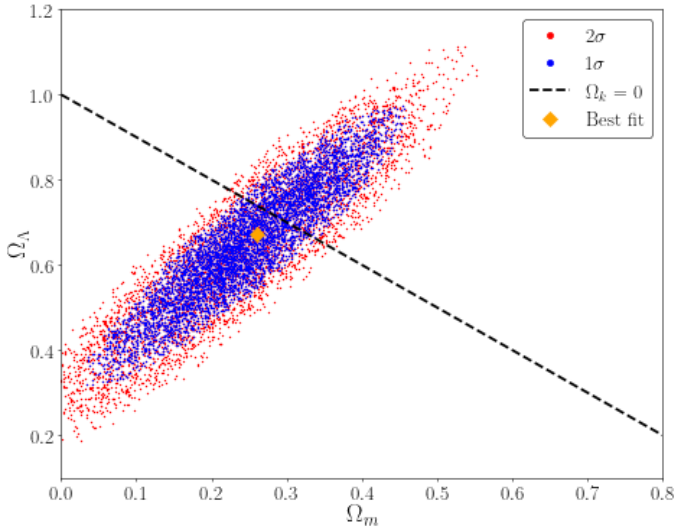

Fig. 7. Confidence regions of Ω_{m0} and $\Omega_{\Lambda 0}$ obtained from fitting the supernova data. The best fit parameter values are shown in the plot, as well as the configurations that would give a flat Universe.

With the fitted parameters, we can solve the background cosmology once again, and compute the resulting luminosity distance. The result is shown in Fig. 9, where the previous result from Fig. 6 is included for comparison purposes. The simulation with the best fit parameters yields a luminosity distance function that is much more consistent with data. However, there is still some discrepancy at lower redshift, but the associated data points in this regime have large uncertainties.

There are three important periods we have discussed, the times of matter-radiation equality, acceleration onset and matter-dark energy equality. The times when these incidents occur are listed in table 2.3.3, in terms of x, redshift z and cosmic time t. We also include the age of the Universe today, $t_0 \equiv t(x = 0)$, and the conformal time today, η_0/c.

	Matter-radiation equality $\Omega_m = \Omega_r$	Acceleration onset $\ddot{a} = 0$	Matter-dark energy equality $\Omega_m = \Omega_\Lambda$
x	−8.132	−0.487	−0.256
z	3400.460	0.627	0.291
t [Gyr]	$5.099 \cdot 10^{-5}$	7.750	10.372

Age of Universe today: $t_0 = 13.848$ Gyr

Conformal time today: $\eta_0/c = 46.284$ Gyr

Table 1. Important times during the evolution of the Universe, expressed in terms of x, redshift and cosmic time. In the last two rows we also present today's time values

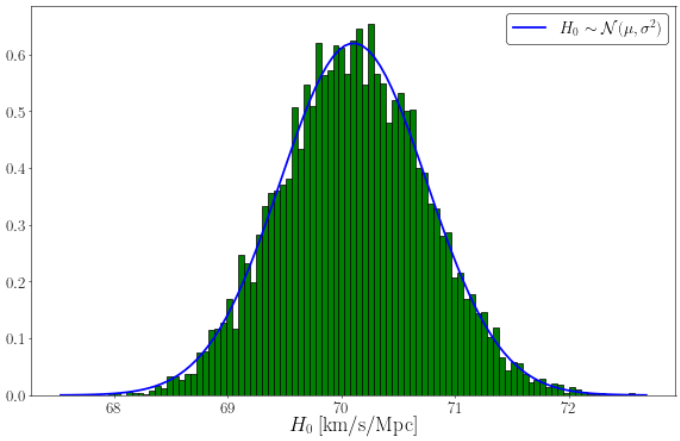

Fig. 8. Posterior PDF of H_0. The histogram shows the sampled values, while the blue curve is the corresponding normal distribution obtained from the mean and variance of the data.

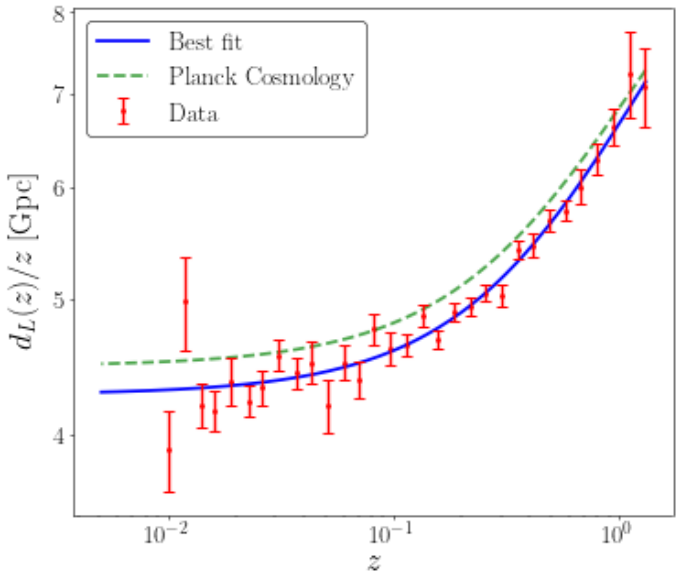

Fig. 9. The luminosity dinstance function obtained from the best fit values of C (blue line), compared with the result from the Planck cosmology (dashed green line), which is also shown in Fig. 6.

3. Milestone II

Having successfully implemented the background cosmology, the next step in developing our model is to include interactions between particles. After the Big Bang, the early universe was highly ionized. Due to Thompson scattering, photons were strongly coupled to baryons. As the Universe expanded, and the temperature dropped, neutral atoms were able to form, and the photons were able to escape from the plasma. These are the CMB photons we observe today. The period where neutral atoms formed is called recombination, and will be the main topic of this section. Our goal is to compute the number density of free electrons in the Universe, and use this to estimate when recombination occurred. The evolution of free electrons will affect both structure formation and the resulting power spectrum of the CMB photons, as we will study later.

We will use the Saha and Peebles equation to compute the electron number density, and use this to compute the optical depth. From the optical depth, we will compute the so-called *visibility function*. Citations?

Write about natural units.

The code for this milestone can be found on my GitHub repository: `https://github.com/Vikenes/AST5220/tree/main/projects/milestone2`

3.1. Theory

3.1.1. Optical depth and visibility function

Write about the basics of optical depth.

The optical depth is defined in terms of the scale factor, a, as

$$\tau(\eta) = \int_{\eta}^{\eta_0} \mathrm{d}\eta' \, n_e \sigma_T a, \tag{33}$$

where $n_e(\eta)$ is the electron number density,

$$\sigma_T = \frac{8\pi\alpha^2}{3m_e^2} = 6.6524587158 \cdot 10^{-29}\ \mathrm{m}^2 \tag{34}$$

is the Thompson cross-section and a is the scale factor. α is the fine-structure constant and m_e is the electron mass. Using Eq. (14), we can rewrite Eq. (33) as a differential equation

$$\frac{\mathrm{d}\tau}{\mathrm{d}x} = -\frac{n_e \sigma_T}{H}, \tag{35}$$

which we will solve numerically. The initial condition is $\tau(x = 0) = 0$.

From the optical depth, we obtain the so-called *visibility function*, which is defined as

$$\tilde{g}(x) = -\tau' e^{-\tau}, \tag{36}$$

which is normalized as

$$\int_{-\infty}^{0} \mathrm{d}x\, \tilde{g}(x) = 1. \tag{37}$$

The normalization means that $\tilde{g}(x)$ is a probability distribution, and we may interpret it as the probability of an observed CMB photon today having experienced its last scattering at a time x. Why do we need derivatives? Once we have an expression for $n_e(x)$, we have all the constituents needed to compute τ and $\tilde{g}$.

The visibility function is sharply peaked around the time when recombination takes place (cite?), and the period of recombination is thus often referred to as the surface of last scattering. We therefore have two ways of estimating when photon baryon decoupling occurred, either as the time when the Universe became optically thin, i.e. when $\tau = 1$, or as the peak of the visibility function. (Fix last paragraph later.)

3.1.2. Electron density (working title)

Instead of computing n_e directly, we will compute the fractional electron density

$$X_e \equiv \frac{n_e}{n_H}, \tag{38}$$

where n_H is the proton density. We will neglect Helium and heavier elements, i.e. assume that all baryons are protons, giving

$$n_H = n_b \approx \frac{\rho_b}{m_H} = \frac{\Omega_{b0}\rho_{c0}}{m_H a^3}, \tag{39}$$

where $\rho_{c0} \equiv \frac{H_0^2}{8\pi G}$ is the critical density of the universe today and m_H is the hydrogen mass. We have assumed the small difference between the proton mass and Hydrogen mass to be negligible.

"Derive" Saha?

The Saha equation is given as

$$\frac{X_e^2}{1 - X_e} = \frac{1}{n_b}\left(\frac{m_e T_b}{2\pi}\right)^{3/2} e^{-\epsilon_0/T_b}, \tag{40}$$

where T_b is the temperature of the baryons, and $\epsilon_0 = 13.6\,\mathrm{eV}$ is the Hydrogen ionization energy. The time evolution of the baryon temperature is governed by a differential equation coupled to X_e. However, we will assume that T_b follows the photon temperature, T_γ, evolving as

$$T_b = T_\gamma = T_{\mathrm{CMB}0} e^{-x}. \tag{41}$$

Cite stuff above, and reference to quantities.

$$\frac{\mathrm{d}X_e}{\mathrm{d}x} = \frac{C_r(T_b)}{H}\left[\beta(T_b)(1 - X_e) - n_H \alpha^{(2)}(T_b) X_e^2\right] \tag{42}$$

$$C_r(T_b) = \frac{\Lambda_{2s\to 1s} + \Lambda_\alpha}{\Lambda_{2s\to 1s} + \Lambda_\alpha + \beta^{(2)}(T_b)}, \tag{43a}$$

$$\Lambda_{2s\to 1s} = 8.227\,\mathrm{s}^{-1}, \tag{43b}$$

$$\Lambda_\alpha = H\frac{(3\epsilon_0)^3}{(8\pi)^2 n_{1s}}\,\mathrm{s}^{-1}, \tag{43c}$$

$$n_{1s} = (1 - X_e) n_H\,\mathrm{m}^{-3}, \tag{43d}$$

$$\beta^{(2)}(T_b) = \beta(T_b) e^{3\epsilon_0/4T_b}\,\mathrm{s}^{-1}, \tag{43e}$$

$$\beta(T_b) = \alpha^{(2)}(T_b)\left(\frac{m_e T_b}{2\pi}\right)^3 / 2e^{-\epsilon_0/T_b}\,\mathrm{s}^{-1}, \tag{43f}$$

$$\alpha^{(2)} = \frac{64\pi}{\sqrt{27\pi}}\frac{\alpha^2}{m_e^2}\sqrt{\frac{\epsilon_0}{T_b}}\phi_2(T_b)\,\mathrm{m}^2\,\mathrm{s}^{-1}, \tag{43g}$$

$$\phi_2(T_b) = 0.448 \ln(\epsilon_0/T_b). \tag{43h}$$

Explain how equations are solved, etc.

3.1.3. Sound Horizon (working title)

Before recombination happens, baryons and photons are tightly coupled. For this reason, the baryons and photons behave as if they were a single fluid, and the sound speed of this fluid is given by (citation)

$$c_s = c\sqrt{\frac{R}{3(1 + 3R)}}, \quad R = \frac{4\Omega_{\gamma 0}}{3\Omega_{b0} e^x}, \tag{44}$$

and we see that during radiation domination, we have $c_s \approx c/\sqrt{3}$. After recombination happens, photons will still have a sound speed of $c_s = c/\sqrt{3}$, while the sound speed of baryons will drop. Is the previous sentence obsolete? The total co-moving distance of these sound waves since the Big Bang is given as

$$s(x) = \int_{-\infty}^{x} \frac{\mathrm{d}x' c_s}{\mathcal{H}}. \tag{45}$$

The size of this co-moving distance at recombination is known as the sound horizon, $r_s = s(x_{\mathrm{rec}})$. This allows us to estimate the angular separation of the CMB, over which we may expect there to have been causal contact. Thus, we have an additional ODE to solve,

$$\frac{\mathrm{d}s(x)}{\mathrm{d}x} = \frac{c_s}{\mathcal{H}}, \tag{46}$$

with $s(x_{\mathrm{ini}}) = \frac{c_s(x_{\mathrm{ini}})}{\mathcal{H}(x_{\mathrm{ini}})}$ as the initial condition, following the same reasoning as we did for $\eta'(x)$ in Eq. (15). Relate the sound-horizon to the Power Spectrum as well.

3.2. Implementation details

In order to compute the optical depth and the visibility we must first compute the electron density. At early times all Hydrogen is ionized, and we therefore have $X_e \approx 1$ (equal to?), and X_e can thus be well approximated by the Saha equation in this regime. As X_e decreases, the Saha approximation is no longer valid, and we must resort to the Peebles equation to compute X_e. We compute X_e by first solving the Saha equation, and when $X_e < X_e^{\mathrm{tol}}$ we resort to the Peebles equation, using the preceding value of from the Saha equation as our initial condition.

3.2.1. Solving the Saha Equation

Solving the Saha equation is done by solving a quadratic formula for X_e. At early times, however, the RHS of Eq. (40) will be huge, and may result in numerical errors when we implement the quadratic formula numerically. To avoid this, we use the first order approximation $\sqrt{1+x} \approx 1 + \frac{x}{2}$ for $|x| \ll 1$ at early times. The equation we will solve is thus

$$X_e = \begin{cases} 1, & y > 10^7, \\ \frac{y}{2}\left[-1 + \sqrt{1 + 4/y}\right], & y \leq 10^7, \end{cases} \tag{47}$$

where we have used y as an abbreviation for the RHS of Eq. (40), and omitted the negative solution as X_e is a strictly positive quantity. The exact value of 10^7 is chosen to ensure $X_e \not> 1$.

3.2.2. Solving the Peebles Equation

We will solve the Peebles equation using Saha as the initial condition. To solve Eq. (42) numerically, we follow the same procedure as we did for $\eta(x)$, but for the initial condition we use the final value of X_e that we obtained from the Saha equation. Once X_e is obtained we get $n_e(x)$ from Eq. (38). However, at late times, when the baryon temperature gets low, the exponent term in Eq. (43e) for $\beta^{(2)}(T_b)$ will yield an overflow. However, the exponential factor in $\beta(T_b) \to 0$ results in $\beta^{(2)}(T_b) \to 0$ at these temperatures. To avoid numerical errors, we therefore compute

$$\beta^{(2)}(T_b) = \begin{cases} 0, & \epsilon_0/T_b > 200, \\ \beta(T_b)e^{3\epsilon_0/4T_b}, & \epsilon_0/T_b \leq 200. \end{cases} \tag{48}$$

3.2.3. Optical depth

With $n_e(x)$ computed, we can solve Eq. (35) for $\tau(x)$ with the aforementioned initial condition of $\tau(x = 0) = 0$. Its derivative, $\tau'(x)$, is given by the ODE and is thus trivial. From this, we get immediately $\tilde{g}(x)$. For the second derivative of τ, we compute it by numerical differentiation of the splines.

3.3. Results

3.3.1. Electron fraction

Table 2. Times when decoupling and recombination occurs, computed from the Peebles equation.

Peebles	x	z	t [Myr]
Decoupling ($\tau = 1$)	-6.98777	1082.3	0.37624
Decoupling max$\{\tilde{g}(x)\}$	-6.98534	1079.67	0.37778
Recombination	-6.98549	1079.83	0.37769

Table 3. Times when decoupling and recombination occurs, computed from the Saha equation.

Saha	x	z	t [Myr]
Decoupling ($\tau = 1$)	-7.15809	1283.46	0.28205
Decoupling max$\{\tilde{g}(x)\}$	-7.15485	1279.3	0.28361
Recombination	-7.14035	1260.87	0.29069

This is given in table 2

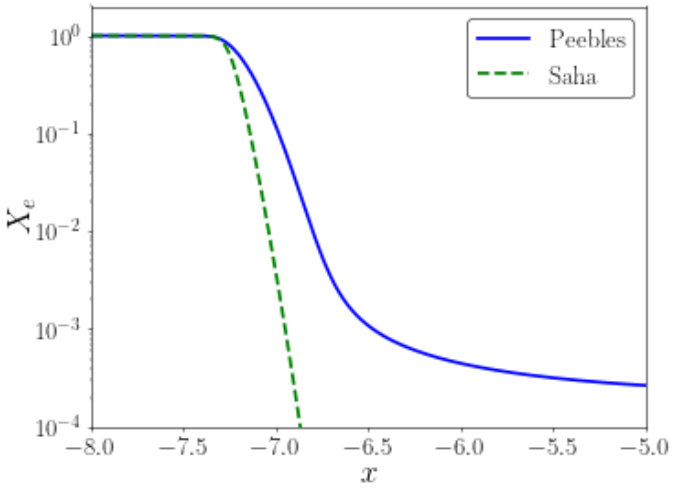

Fig. 10. Free electron fraction computed from the Saha equation only (dashed green curve) and from the Peebles equation (solid blue curve), where the Saha equation was used at early times, until $X_e < 0.99$.

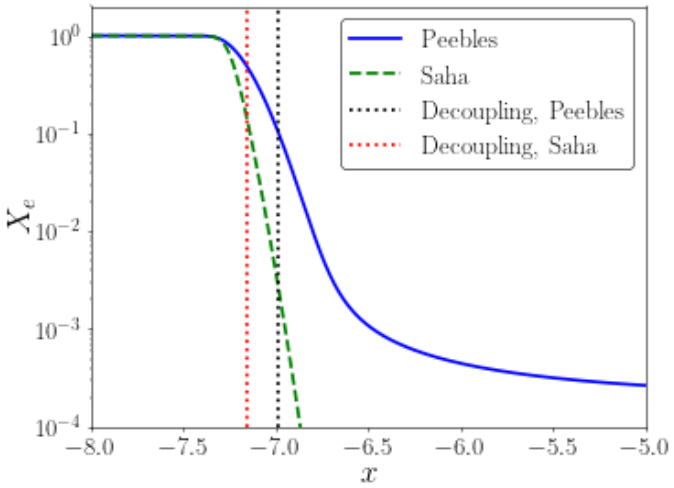

Fig. 11. Free electron fraction computed from the Saha equation only (dashed green curve) and from the Peebles equation (solid blue curve), where the Saha equation was used at early times, until $X_e < 0.99$. The decoupling time, i.e. when $\tau = 1$, is shown for both the Saha solution (dotted red curve), and for the Peebles solution (dotted black curve).

4. Milestone III

Some introduction about what it is all about.

4.1. Theory

The theory behind this milestone.

4.2. Implementation details

Something about the numerical work.

4.3. Results

Show and discuss the results.

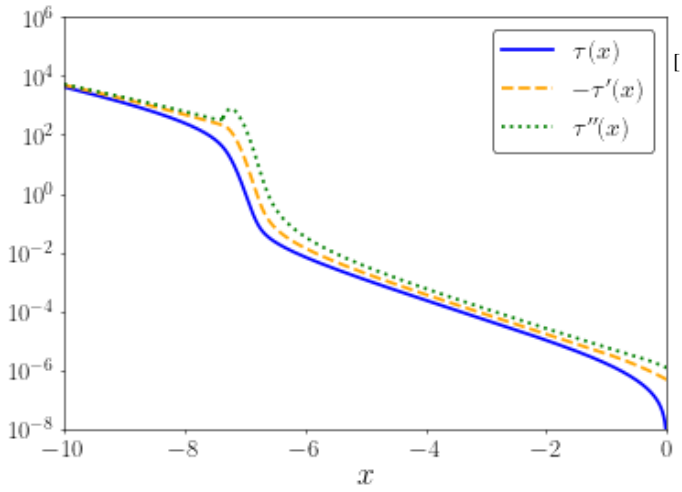

Fig. 12. The optical depth, $\tau(x)$ and its two first derivatives with respect to x.

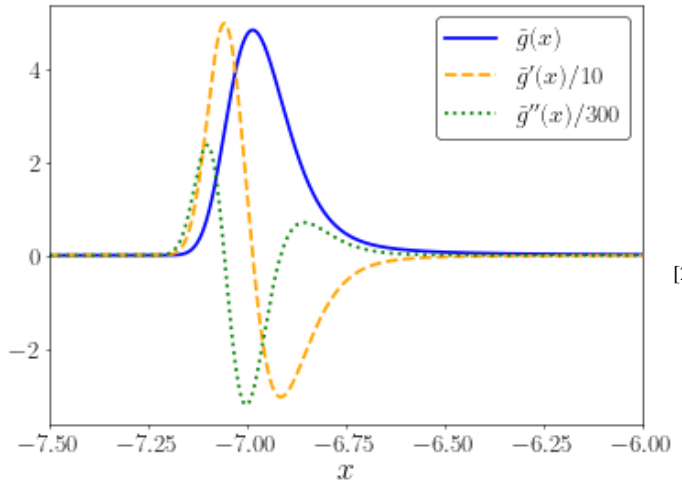

Fig. 13. The visibility function, $\tilde{g}(x)$ (solid curve), and its derivatives, $\tilde{g}'(x)/10$ (dashed curve) and $\tilde{g}''(x)/300$ (dotted curve). The derivatives have been scaled in order to view them all in the same plot.

5. Milestone IV

Some introduction about what it is all about.

5.1. Theory

The theory behind this milestone.

5.2. Implementation details

Something about the numerical work.

5.3. Results

Show and discuss the results.

6. Conclusions

Write a short summary and conclusion in the end.

Acknowledgements. I thank my mom for financial support!

References

[1] Planck Collaboration, N. Aghanim, Y. Akrami, M. Ashdown, J. Aumont, C. Baccigalupi, M. Ballardini, A. J. Banday, R. B. Barreiro, N. Bartolo, S. Basak, R. Battye, K. Benabed, J. P. Bernard, M. Bersanelli, P. Bielewicz, J. J. Bock, J. R. Bond, J. Borrill, F. R. Bouchet, F. Boulanger, M. Bucher, C. Burigana, R. C. Butler, E. Calabrese, J. F. Cardoso, J. Carron, A. Challinor, H. C. Chiang, J. Chluba, L. P. L. Colombo, C. Combet, D. Contreras, B. P. Crill, F. Cuttaia, P. de Bernardis, G. de Zotti, J. Delabrouille, J. M. Delouis, E. Di Valentino, J. M. Diego, O. Doré, M. Douspis, A. Ducout, X. Dupac, S. Dusini, G. Efstathiou, F. Elsner, T. A. Enßlin, H. K. Eriksen, Y. Fantaye, M. Farhang, J. Fergusson, R. Fernandez-Cobos, F. Finelli, F. Forastieri, M. Frailis, A. A. Fraisse, E. Franceschi, A. Frolov, S. Galeotta, S. Galli, K. Ganga, R. T. Génova-Santos, M. Gerbino, T. Ghosh, J. González-Nuevo, K. M. Górski, S. Gratton, A. Gruppuso, J. E. Gudmundsson, J. Hamann, W. Handley, F. K. Hansen, D. Herranz, S. R. Hildebrandt, E. Hivon, Z. Huang, A. H. Jaffe, W. C. Jones, A. Karakci, E. Keihänen, R. Keskitalo, K. Kiiveri, J. Kim, T. S. Kisner, L. Knox, N. Krachmalnicoff, M. Kunz, H. Kurki-Suonio, G. Lagache, J. M. Lamarre, A. Lasenby, M. Lattanzi, C. R. Lawrence, M. Le Jeune, P. Lemos, J. Lesgourgues, F. Levrier, A. Lewis, M. Liguori, P. B. Lilje, M. Lilley, V. Lindholm, M. López-Caniego, P. M. Lubin, Y. Z. Ma, J. F. Macías-Pérez, G. Maggio, D. Maino, N. Mandolesi, A. Mangilli, A. Marcos-Caballero, M. Maris, P. G. Martin, M. Martinelli, E. Martínez-González, S. Matarrese, N. Mauri, J. D. McEwen, P. R. Meinhold, A. Melchiorri, A. Mennella, M. Migliaccio, M. Millea, S. Mitra, M. A. Miville-Deschênes, D. Molinari, L. Montier, G. Morgante, A. Moss, P. Natoli, H. U. Nørgaard-Nielsen, L. Pagano, D. Paoletti, B. Partridge, G. Patanchon, H. V. Peiris, F. Perrotta, V. Pettorino, F. Piacentini, L. Polastri, G. Polenta, J. L. Puget, J. P. Rachen, M. Reinecke, M. Remazeilles, A. Renzi, G. Rocha, C. Rosset, G. Roudier, J. A. Rubiño-Martín, B. Ruiz-Granados, L. Salvati, M. Sandri, M. Savelainen, D. Scott, E. P. S. Shellard, C. Sirignano, G. Sirri, L. D. Spencer, R. Sunyaev, A. S. Suur-Uski, J. A. Tauber, D. Tavagnacco, M. Tenti, L. Toffolatti, M. Tomasi, T. Trombetti, L. Valenziano, J. Valiviita, B. Van Tent, L. Vibert, P. Vielva, F. Villa, N. Vittorio, B. D. Wandelt, I. K. Wehus, M. White, S. D. M. White, A. Zacchei, and A. Zonca. Planck 2018 results. VI. Cosmological parameters. *A&A*, 641:A6, September 2020. .

[2] M. Betoule, R. Kessler, J. Guy, J. Mosher, D. Hardin, R. Biswas, P. Astier, P. El-Hage, M. Konig, S. Kuhlmann, J. Marriner, R. Pain, N. Regnault, C. Balland, B. A. Bassett, P. J. Brown, H. Campbell, R. G. Carlberg, F. Cellier-Holzem, D. Cinabro, A. Conley, C. B. D'Andrea, D. L. DePoy, M. Doi, R. S. Ellis, S. Fabbro, A. V. Filippenko, R. J. Foley, J. A. Frieman, D. Fouchez, L. Galbany, A. Goobar, R. R. Gupta, G. J. Hill, R. Hlozek, C. J. Hogan, I. M. Hook, D. A. Howell, S. W. Jha, L. Le Guillou, G. Leloudas, C. Lidman, J. L. Marshall, A. Möller, A. M. Mourão, J. Neveu, R. Nichol, M. D. Olmstead, N. Palanque-Delabrouille, S. Perlmutter, J. L. Prieto, C. J. Pritchet, M. Richmond, A. G. Riess, V. Ruhlmann-Kleider, M. Sako, K. Schahmaneche, D. P. Schneider, M. Smith, J. Sollerman, M. Sullivan, N. A. Walton, and C. J. Wheeler. Improved cosmological constraints from a joint analysis of the SDSS-II and SNLS supernova samples. *A&A*, 568:A22, August 2014. .

[3] Scott Dodelson and Fabian Schmidt. *Modern Cosmology*. Academic Press, 2020. .

[4] M et al Galassi. *GNU scientific library reference manual*. Network Theory Ltd., 2009. ISBN 0954612078.

Appendix A: Fiducial parameters

The parameter values we use in this report are

$$
\begin{aligned}
h &= 0.67,\\
T_{\mathrm{CMB0}} &= 2.7255\,\mathrm{K},\\
N_{\mathrm{eff}} &= 3.046,\\
\Omega_{b0} &= 0.05,\\
\Omega_{\mathrm{CDM0}} &= 0.267,\\
\Omega_{k0} &= 0,\\
\Omega_{\nu 0} &= N_{\mathrm{eff}} \cdot \frac{7}{8}\left(\frac{4}{11}\right)^{4/3} \Omega_{\gamma 0},\\
\Omega_{\Lambda 0} &= 1 - (\Omega_{k0} + \Omega_{b0} + \Omega_{\mathrm{CDM0}} + \Omega_{\gamma 0} + \Omega_{\nu 0}),\\
n_s &= 0.965,\\
A_s &= 2.1 \cdot 10^{-9},\\
Y_p &= 0.245,\\
z_{\mathrm{reion}} &= 8,\\
\Delta z_{\mathrm{reion}} &= 0.5,\\
z_{\mathrm{Hereion}} &= 3.5,\\
\Delta z_{\mathrm{Hereion}} &= 0.5,
\end{aligned}
\tag{A.1}
$$